PMU-based Real-time Distribution System State Estimation Considering Anomaly Detection, Discrimination and Identification

Veerakumar, Nidarshan; Ćetenović, Dragan ; Kongurai, K.; Popov, M.; Jongepier, Arjen; Terzija, Vladimir

DOI
10.1016/j.ijepes.2022.108916

Publication date
2022

Document Version
Final published version

Published in
International Journal of Electrical Power & Energy Systems

Electrical Power and Energy Systems 148 (2023) 108916

Contents lists available at ScienceDirect

International Journal of Electrical Power and Energy Systems

journal homepage: www.elsevier.com/locate/ijepes

PMU-based Real-time Distribution System State Estimation Considering Anomaly Detection, Discrimination and Identification

Nidarshan Veerakumar [a], Dragan Ćetenović [b,c], Krit Kongurai [a], Marjan Popov [a,*], Arjen Jongepier [d], Vladimir Terzija [e]

[a] Delft University of Technology, Faculty of EEMCS, Mekelweg 4, Delft, 2628CD, The Netherlands
[b] The Department of Electrical & Electronic Engineering, The University of Manchester, Manchester, United Kingdom
[c] University of Kragujevac, Faculty of Technical Sciences Čačak, Svetog Save 65, 32000 Čačak, Serbia
[d] Stedin Group B.V., Blaak 8, Rotterdam, 3011TA, The Netherlands
[e] Key Laboratory of Power System Intelligent Dispatch and Control of Ministry of Education, School of Electrical Engineering, Shandong University, Jinan, 250061, China

ARTICLE INFO

Keywords:
Anomaly detection
Discrimination and identification
Bad data
Extended kalman filter
Forecasting-aided state estimation
Real time digital simulator
Sudden load change

ABSTRACT

In this paper, a real-time state estimation platform for distribution grids monitored by Phasor Measurement Units (PMUs) is developed, tested, and validated using Real Time Digital Simulator (RTDS). The developed platform serves as a proof-of-concept for potential implementation in an existing 50 kV ring network of the Dutch distribution utility Stedin medium voltage distribution grid located in the southwest (Zeeland area) of the Netherlands. To catch up with the fast sampling rates of PMUs, the platform incorporates computationally efficient techniques for state estimation and detection, discrimination and identification of anomalies like bad data and sudden load changes. Forecasting Aided State Estimation has been utilized to enable measurement innovations needed for fast anomaly detection, discrimination, and identification, whilst the Extended Kalman Filter (EKF) algorithm is selected to provide fast state forecasting and filtering. The platform has been tested under various normal and abnormal operating conditions considering different statistical properties of measurement noise as well as different bad data and sudden load change scenarios. To demonstrate advantages and disadvantages for embedding EKF into the platform, EKF is compared with Unscented Kalman Filter (UKF) in terms of estimation accuracy, computational efficiency, and compatibility with the module for anomaly detection, discrimination, and identification. The results of extensive simulations provide good hints about the feasibility of PMU-based real-time state estimation for the Stedin distribution grid.

1. Introduction

State estimation (SE) plays an important role in monitoring and control of power systems by providing reliable estimates of the system states. They represent the backbone of any Energy/ Distribution Management System. In the past several decades, SE of transmission networks was prioritized. This resulted in the advancement of solutions during the time. On the other hand, the SE of distribution networks remained in the background for a long time since these grids have been mainly radial with uni-directional power flows making classical monitoring and control fairly sufficient. To ensure the optimal integration of intermittent and volatile renewable generation and to maximize the grid hosting capacity, more sophisticated monitoring and control of distribution networks is needed. This calls for developing advanced Distribution System State Estimation (DSSE) approaches. At the same time, the practicability of the existing approaches against electrical and/or communication disturbances in real-life distribution networks is equally important to be validated.

SE in power systems as a subject had evolved from 1970 when it was proposed for the first time by Schweppe [1]. Yet only a few SE models were worthy enough to be built in real-world settings. Classical weighted least square (WLS) based static state estimation (SSE) matches the features of transmission networks [1,2]. However, due to high redundancy requirements and sensitivity to missing and bad data, WLS SSE encountered resentment in distribution networks [3]. The drawbacks of WLS SSE could be overcome by using Forecasting-Aided State Estimation (FASE) which consists of two stages: prediction stage and estimation stage. State predictions can be considered as an additional set of measurements improving the overall redundancy. FASE usually employs different variants of classical Kalman filter capable to handle

* Corresponding author.
E-mail address: m.popov@tudelft.nl (M. Popov).

https://doi.org/10.1016/j.ijepes.2022.108916
Received 22 August 2022; Accepted 16 December 2022

distribution system nonlinearities: Extended Kalman Filter, Unscented Kalman Filter, Ensemble Kalman Filter, Cubature Kalman Filter, to name a few [3–6]. Each variant has its advantages and disadvantages, so the choice is usually influenced by the compromise between estimation accuracy, computational efficiency and robustness to different types of anomalies. As compared to others, Extended Kalman Filter (EKF) usually demonstrates better computational efficiency which is essential for real-time applications [7–9]. Although other variants might cope better with high degree of nonlinearities, EKF still works well in a 'mild' nonlinear environment showing high accuracy for quasi-linear systems [7,8].

Thanks to the benefits of the process model, FASE can achieve more accurate estimates than SSE in normal operation, i.e., in the absence of bad data (BD) when the system operation point changes slowly enough over the time. The operation point of real distribution networks can change abruptly due to sudden load change (SLC), large uncertainties in the output power of distributed renewable energy sources (RES), as well as due to network reconfiguration. This can temporarily spoil the accuracy of FASE until new quasi-steady state operation point is reached, because process noise level will increase during the transition [10,11]. Apart from this, telemetric failures cause BD. If left unattended, BD can produce misleading system states [12,13], introducing input errors for other centralized control applications (e.g., Economic Dispatch and Contingency Analysis Programs). False Data Injection Attack, as a sort of smartly organized BD, threatens the FASE progressively as the distribution network evolves to a cyber–physical system. It is hard to completely prevent the occurrence of any kind of anomaly; however, anomaly should be detected anytime it appears in order to avoid negative effects on the estimator's performance. In general, there have been many attempts to detect anomaly presence, discriminate between different types of anomalies and identify the origin of anomaly in power systems; starting from pioneering papers like [14–16], through later work [10,17,18], all the way to the most recent published research [11–13,19,20]. Yet, Anomaly Detection, Discrimination, and Identification (ADDI) faced a lot of troubles in distribution networks due to a lack of telemetry. Reliable ADDI requires sufficient measurement redundancy which real-life distribution networks do not possess. Therefore, many ADDI methods for transmission networks easily fail at the distribution level. In addition, most traditionally used ADDI methods rely on measurement residuals. To enable ADDI this way, it is required to execute state estimation at least once but sometimes even more before the final estimation stage. Those ADDI methods would not be the best choice for real-time applications because they increase the computational burden.

For a long time, monitoring of real-life distribution networks was based on Supervisory Control and Data Acquisition (SCADA) systems. Modern SCADA delivers the measurements with sampling rates of 2–4 s [7]. With the application of synchrophasors standardized in 2005 through IEEE C37.118 standard, 50(60) samples/second time-aligned phasor measurement unit (PMU) data acquisition became possible [21]. High sampling rates and accuracy of PMUs created an opportunity for realization of many real-time applications [22], however it also brought about new challenges. For the sake of clarity, the application is considered to run in real-time when its execution time is shorter or equal to the selected time step. This time step is usually influenced by the time constant of physical phenomena to be captured and/or by sampling rates of collected measurements. For the SE driven by PMUs this requires very fast execution, including both ADDI and final estimation execution. The practical utilization of PMUs in real-life distribution networks is still rare due to (a) high PMU price, (b) higher number of nodes as compared to transmission networks, and (c) lower priorities for monitoring and control as compared to transmission networks [23,24]. Although there is a lot of work on PMU based DSSE reported in the literature, assumptions are usually made regarding the amount of PMUs implemented in DSSE and regarding their placement in the network [25–28]. Distribution networks where PMU based DSSE has been tested are usually benchmark distribution test systems (IEEE, UK test systems, etc.) [29–31]. Although examples of small smart-grid distribution networks built up at University Campuses are tested before [32], there is no work reported on real-life distribution network totally covered with PMU measurements.

In order to provide the required confidence for implementation into the control center, the performance of PMU-based DSSE should to be validated under a simulated real-time environment. Real-Time Digital Simulator (RTDS) is able to solve the power system equations close to 25–50 μs, which can realistically represent conditions of a real-life network [33]. Besides, it provides PMU firmware that can communicate voltage and current phasors, power injections and power flows to any external device outside the simulation platform. In [34], preliminary works on how RTDS is utilized to obtain real-time view of the network's state using state estimation is explored. In [35], the RTDS and data acquisition platform is used for the validation of real-time dynamic state estimation and further informed decisions on optimal PMU placements is made on IEEE 39 Bus system. In [36,37], RTDS is used to validate the application of state estimation on 14 bus test microgrid. For SE studies, in general, RTDS simulated PMU streams are time-stamped at an external phasor data concentrator (PDC) and utilized as true measurements in a measurement vector. Since these PMU measurements are the most *close-to-real-life* streams that can be generated for simulation at 50(60) samples/second, a DSSE capable of working under these high reporting rate conditions can be directly deployed in control centers for online power system states visualization [38]. Moreover, with RTDS, the power system's behavior can be simulated under various transient and load profiles driven quasi-steady state (QSS) conditions which can be used to assess the robustness of PMU-based DSSE and ADDI algorithms. Since PMU streams are acquired from the external platform, there is also an opportunity to artificially inject BD at PDC level. This can be further used to challenge ADDI algorithms and check for their resilience against BD.

In this paper, we use RTDS to test and validate the performance of PMU-based DSSE for potential implementation into the control center of 50 kV Stedin network located in the Zeeland area of the Netherland. Zeeland 50 kV ring network is a real-life medium-voltage distribution network with a high PMU redundancy. To the best of authors knowledge, this is the first example of a real-life distribution network covered with a significant amount of PMUs where the number and the locations of PMUs are not assumed but correspond to a real situation in the site. For the successful validation of DSSE, we identified three necessary requirements: firstly, a real-time simulation and data acquisition platform capable of mimicking real-life event scenarios; secondly, an ADDI module acting as a screening stage to ensure measurement quality; finally, an efficient DSSE capable of operating within PMU sampling rate. Hence, the paper focuses on achieving this workflow to realize an efficient real-time state estimator.

We consider that abrupt changes in a system operation point are caused by SLC, whilst BD appears due to the sensor and/or communication failures. Network topology changes and sophisticated malicious data attacks are not in the scope of this paper. Consequently, ADDI methodology is selected to screen anomalies like SLC and BD. Two of the pre-estimation schemes from [3,14] have been tested for the detection and discrimination of SLC and BD. Next, they are tested to identify either the PMU placed at the bus with the disturbed load or the PMU corrupted with BD. Lastly, countermeasures are applied based on the type of anomaly.

In this paper, EKF FASE is selected as an estimation algorithm in the PMU-based DSSE. By utilizing FASE instead of SSE, the redundancy is additionally increased in an artificial way. The redundant information enables more accurate estimates during normal operation and facilitates ADDI under abnormal conditions. FASE takes care of providing measurement innovations to be used in ADDI instead of measurement residuals. In this way, the screening stage requires less time because time consuming post-estimation schemes can be avoided. This is essentially important because SE scheme coupled with the

ADDI should consume lower computational time than that with the fast refresh rate of PMUs. Finally, the estimation stage also requires a computationally efficient algorithm that is enabled by deploying EKF. EKF computational efficiency is demonstrated against Unscented Kalman Filter (UKF).

This paper is organized as follows: Section 2 introduces the FASE fundamentals and addresses the concepts of EKF-based FASE technique; Section 3 presents the ADDI methods along with counteractions; Section 4 describes the test set-up, thresholds and simulation settings; Section 5 presents the simulation results obtained under the influence of various noise and network conditions, and finally Section 6 concludes the paper.

2. FASE EKF fundamentals

2.1. Process model

The formulation of the process model in the state space is as following:

$$\boldsymbol{x}_{k+1} = \boldsymbol{F}_k \boldsymbol{x}_k + \boldsymbol{g}_k + \boldsymbol{w}_k \tag{1}$$

where $\boldsymbol{x}$ is n × 1 state vector composed of three-phase nodal voltages in polar coordinates; $\boldsymbol{F}$ and $\boldsymbol{g}$ are n × n state transition matrix and n × 1 state transition vector, respectively, updated using Holt's linear exponential smoothing [39]; $\boldsymbol{w}$ is n × 1 white Gaussian process noise with zero mean and n × n covariance matrix $\boldsymbol{Q}$; n is number of states; index k denotes the time sample.

2.2. Measurement model

The measurement function is given as:

$$\boldsymbol{z}_k = \boldsymbol{h}(\boldsymbol{x}_k) + \boldsymbol{e}_k \tag{2}$$

where $\boldsymbol{z}$ is m × 1 measurement vector; $\boldsymbol{h}$ is m × 1 nonlinear vector function representing the link between the measurements and the states; $\boldsymbol{e}$ is m × 1 white Gaussian measurement noise with zero mean and m × m covariance matrix $\boldsymbol{R}$; m is the number of measurements. The measurement vector $\boldsymbol{z}$ is composed of bus voltages and branch currents measured by PMUs in polar coordinates, pseudo measurements of non-zero active and reactive bus power injections and virtual measurement of zero bus injections.

The performance of every type of Kalman filter is influenced by the ratio between $\boldsymbol{Q}$ and $\boldsymbol{R}$ [26,40]. For real-world distribution networks the true value of $\boldsymbol{Q}/\boldsymbol{R}$ ratio is not available and should be estimated. For most cases, $\boldsymbol{R}$ can be defined easier and closer to the true one ($\boldsymbol{R}$ depends on class of accuracy of measurement devices which is usually known). Then, using defined $\boldsymbol{R}$, optimal $\boldsymbol{Q}$ for quasi-steady state operation can be defined through offline analysis of this operation mode [41].

2.3. Extended Kalman filter

Based on (1) and (2), EKF performs SE by utilizing the following set of equations:

$$\boldsymbol{x}_{k+1}^{-} = \boldsymbol{F}_k \boldsymbol{x}_k^{+} + \boldsymbol{g}_k \tag{3}$$

$$\boldsymbol{P}_{k+1}^{-} = \boldsymbol{F}_k \boldsymbol{P}_k^{+} \boldsymbol{F}_k^{T} + \boldsymbol{Q}_k \tag{4}$$

$$\boldsymbol{\upsilon}_{k+1} = \boldsymbol{z}_{k+1} - \boldsymbol{h}(\boldsymbol{x}_{k+1}^{-}) \tag{5}$$

$$\boldsymbol{S}_{k+1} = \boldsymbol{H}_{k+1} \boldsymbol{P}_{k+1}^{-} \boldsymbol{H}_{k+1}^{T} + \boldsymbol{R}_{k+1} \tag{6}$$

$$\boldsymbol{K}_{k+1} = \boldsymbol{P}_{k+1}^{-} \boldsymbol{H}_{k+1}^{T} \boldsymbol{S}_{k+1}^{-1} \tag{7}$$

$$\boldsymbol{x}_{k+1}^{+} = \boldsymbol{x}_{k+1}^{-} + \boldsymbol{K}_{k+1} \boldsymbol{\upsilon}_{k+1} \tag{8}$$

$$\boldsymbol{P}_{k+1}^{+} = [\boldsymbol{I} - \boldsymbol{K}_{k+1} \boldsymbol{H}_{k+1}] \boldsymbol{P}_{k+1}^{-} \tag{9}$$

where $\boldsymbol{x}^{-}(\boldsymbol{x}^{+})$ and $\boldsymbol{P}^{-}(\boldsymbol{P}^{+})$ are forecasted (estimated) state vector and its covariance matrix, respectively; $\boldsymbol{\upsilon_{k+1}}$ is the innovation vector; $\boldsymbol{S}_{k+1}$ is the innovation covariance matrix; $\boldsymbol{H}_k$ is the Jacobian matrix; $\boldsymbol{K}_{k+1}$ is the Kalman gain; $\boldsymbol{I}$ is the identity matrix. EKF can be initialized using estimation results of WLS at time k=0 to get initial estimated state vector $\boldsymbol{x}_0^{+}$ and its covariance matrix $\boldsymbol{P}_0^{+}$ [42].

By taking into account that the real-time state estimation in our work mostly utilizes linear PMU measurements and a few nonlinear pseudo/virtual measurements, only few elements in the Jacobian matrix should be updated over time whilst most of the entries will be constant. This eliminates the risk of high computational burden making EKF a suitable choice for a proof-of-concept.

3. Anomaly detection, discrimination and identification

By using the prediction results of EKF FASE, in this paper the following two methods are adopted for ADDI: the conventional innovation analysis method [14], and the improved innovation analysis method [3]. For the sake of clarity, the detection refers to the determination of the anomaly presence, the discrimination is the classification of the detected anomaly according to its type, whilst the identification is the procedure of finding out the origin of the anomaly in order to properly counter it and make the SE remain unbiased. Anomalies that will be addressed in this paper are SLC and BD, where BD considers only gross errors in the recorded measurements. The incorrect topology information or errors contained in the network parameters are more complicated to deal with [15]. Consequently, they are not under the scope of this paper. We also neglect the possibility of having BD at the same time with SLC given that the probability of such an event happening is quite low.

Regardless ADDI method adopted, the presence of the anomaly is detected using the largest normalized innovation test (Section 3.1). The skewness of normalized innovation distributions (Section 3.2) and/or the skewness of the largest normalized innovation ratio (Section 3.3) are used to discriminate between BD and SLC, depending on the adopted ADDI method. The identification stage has been briefly described in Section 3.4. The adopted ADDI methods are presented in Sections 3.5–3.6. Finally, the anomalies are managed suitably as per Section 3.7.

3.1. Largest normalized innovation test

In order to detect the anomaly presence, an innovation analysis is conducted. It is one of the pre-estimation techniques for the anomalies' processing [15,43]. The principle is based on the statistical characteristics of the normalized innovation (NI) vector $\boldsymbol{\tau}$ whose ith element is defined as the following:

$$\boldsymbol{\tau}_k(i) = \frac{\boldsymbol{\upsilon}_k(i)}{\sqrt{\boldsymbol{S}_k(i,i)}} \tag{10}$$

Once NIs are calculated, the largest normalized innovation (LNI) can be determined as $LNI_k = \max_i |\boldsymbol{\tau}_k(i)|$ and compared with the threshold $\boldsymbol{\gamma}$ to check for the presence of anomalies. If $LNI_k > \boldsymbol{\gamma}$, the presence of anomalies is detected.

The choice of the detection threshold $\boldsymbol{\gamma}$ depends on the statistical properties of the noise. For a Gaussian measurement and a process noise with known standard deviations, $\boldsymbol{\gamma}$ setting is still influenced by $\boldsymbol{Q}/\boldsymbol{R}$ ratio [41]. Although measurement standard deviations can be known fairly, the knowledge of process noise standard deviations cannot be so reliable because process noise varies over time (even in a quasi-steady state). Therefore, offline simulations of quasi-steady state have to be

run for each particular test network and measurement configuration in order to establish γ that clearly distinguishes abnormal from normal operation [14]. This is even more necessary when noise is non-Gaussian distributed.

3.2. Skewness of NI distributions

The skewness is a measure of an asymmetry level in the distributions. When the skewness is closer to zero value, the distribution is more symmetrical and vice versa. This property for NIs distribution can be used to discriminate between BD and SLC since the presence of BD may shift the NIs distribution from being symmetrical, whilst under SLC the distribution will remain symmetrical. The skewness is defined as [3,14,39]:

$$\psi_k = M_{3,k}/\rho_k^3 \tag{11}$$

where M_3 is the third central moment; ρ is the standard deviation of the distribution. They can be obtained as follows:

$$M_{3,k} = E\left\{(\boldsymbol{\tau}_k)^{.*3}\right\} - 3\mu_k E\left\{(\boldsymbol{\tau}_k)^{.*2}\right\} + 2\mu_k^3 \tag{12}$$

$$\rho_k^2 = E\left\{(\boldsymbol{\tau}_k)^{.*2}\right\} - \mu_k^2 \tag{13}$$

$$\mu_k = E\left\{\boldsymbol{\tau}_k\right\} \tag{14}$$

where the operator $. * b$ is element-wise exponentiation for a vector base with the power b. The calculated skewness is tested for a discrimination threshold ζ. If $|\psi_k| > \zeta$, the anomaly is recognized as BD; otherwise, the system is affected by SLC as depicted. The discrimination threshold ζ depends on the system and can be determined by offline simulations for the anomalies [14,39].

Since it measures the asymmetry level of the distributions, the skewness is convenient to discriminate between BD and SLC when the noises follow symmetrical distributions. However, the discrimination capability will be questionable if the noise distribution is asymmetrical (like in the case of the Gaussian Mixture model).

3.3. Skewness to the largest NI ratio

Apart from the skewness of NI distributions, it is reported in [3] that the skewness to the largest NI ratio (SIR), given as:

$$SIR_k = |\psi_k|/LNI_k \tag{15}$$

has a clear threshold to separate BD and SLC. This discrimination threshold is defined as $\mathrm{SIR}_{th} = \min(1/3,\ 3\sigma_{max})$, where σ_{max} is the maximum of the measurement noise standard deviations. If $\mathrm{SIR}_k > \mathrm{SIR}_{th}$, the anomaly is recognized as BD; otherwise, SLC happened.

3.4. Anomaly identification

This step aims to identify the anomaly so that it can be appropriately countered. After the anomaly is discriminated using the skewness of NIs distribution and/or the SIR, an indicator of the suspicion of the observed measurements is created as a set of flagged measurement indexes [5]. When the ith scanned measurement satisfies the condition $\left|\boldsymbol{\tau}_k(i)\right| > \gamma$, the ith index is set to one, indicating that this index is flagged and the corresponding measurement is being suspected. Otherwise, the ith index is set to zero indicating that the corresponding measurement is non-suspected.

If an anomaly is recognized as BD, the PMU measurements corrupted with BD are identified by finding all flagged measurement indexes. If an anomaly is recognized as a SLC, only the PMU measurement associated with the LNI is identified to locate the PMU nearest to the bus with a SLC.

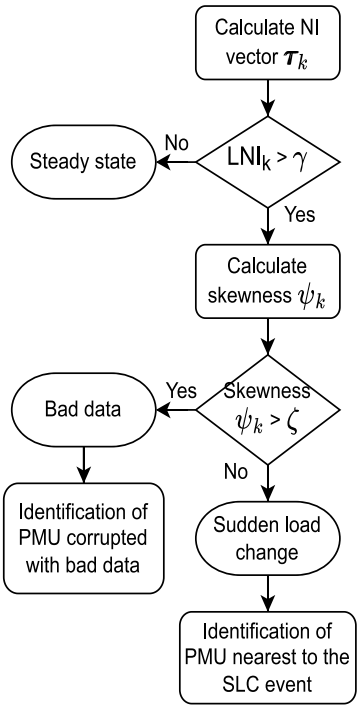

Fig. 1. The flowchart of conventional innovation analysis method (Method 1).

3.5. The conventional innovation analysis method

The conventional innovation analysis method, referred to as Method 1 in this paper, has been used in [3,14,39,44,45]. This method utilizes LNI test and the skewness of NIs distribution ψ_k. The flowchart of Method 1 is presented in Fig. 1.

3.6. The improved innovation analysis method

The second method used in this paper is the improved innovation analysis method, which will be referred to as Method 2. This is proposed in [3] in order to discriminate BD, SLC, and a sudden topology change by using LNI test, the skewness of NIs distribution ψ_k and the SIR index. Note that anomalies like sudden topology changes are not under the scope of this paper. Therefore, the ADDI algorithm from [3] is simplified resulting in the flowchart shown in Fig. 2.

3.7. Countermeasures for detected anomalies

This step aims at countermeasures taken after the ADDI stage. If BD occurs, the identified measurement(s) corrupted with BD is substituted with the corresponding forecasted measurement(s) before executing the EKF filtering process. When SLC occurs, WLS SSE is performed instead of the EKF filtering process because the predictions of EKF are unreliable under SLC. It is ensured that these countermeasures are light enough and provide the most reliable estimates during anomalous conditions without compromising on computational efficiency.

4. Implementation aspects

The implementation of the EKF-based FASE and ADDI algorithm has been carried out using MATLAB R2020b running on an i7-9700 @ 3.00 GHz CPU, 8 GB RAM. The real-time experimental set-up (Section 4.1) simulates the true (actual) measurements. The raw (scanned) measurements for SE are obtained by adding random noises to the true

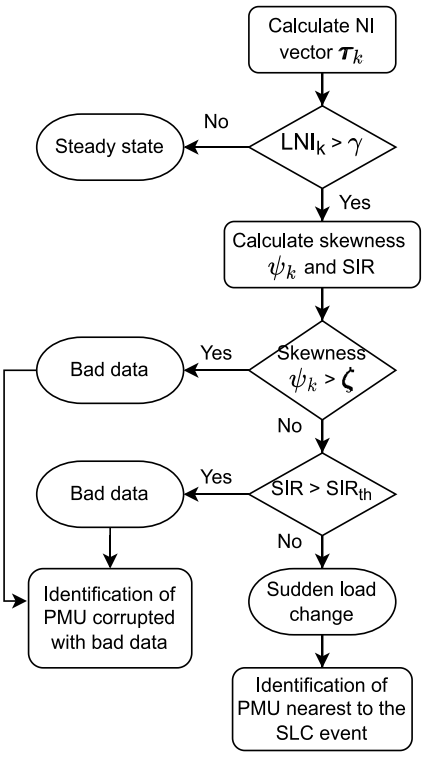

Fig. 2. The flowchart of improved innovation analysis method (Method 2).

measurements. The noises are Gaussian with a zero mean and have uncertainties according to Table 1. Section 4.2 explains the assessment of the measurement and the process noise covariance matrix. Section 4.3 shows the threshold values for the adopted ADDI tests. The estimation performance is evaluated using the indices from Section 4.4.

4.1. Real-time experimental set-up

In this paper, an actual 50 kV ring of a Stedin network located in the southwest (Zeeland area) of the Netherlands is used as a test benchmark. The network topology with the measurement configuration and the power flows are depicted in Fig. 3. The 150 kV busbar (bus 1), which is not covered with PMU, is assumed to be a slack bus with constant voltage over time. For the 50 kV voltage level, there are five PMU voltage measurements at every substation from bus 2 to bus 6, and six PMU current measurements on the three-phase 50 kV cables. Apart from this, pseudo measurements of power injections at their nominal power, and virtual measurements of zero injections are simulated, as shown in Fig. 3, to ensure the full network observability. This work is focused on the estimation of states at buses 1–6, i.e., all 50 kV busbars and 150 kV busbar.

A Real-Time Digital Simulator (RTDS) can simulate physical models in real-time with time steps as low as tens of microseconds. This high precision of the simulator facilitates mimicking the quasi-steady state (QSS) nature of the distribution grid close to real life. Besides, with the integration of intermittent RES, the RTDS is extremely useful to capture the system dynamics driven by power electronics-based RES.

Fig. 4 depicts the laboratory setup designed at TU Delft RTDS laboratory. The PMU data streams of 50 kV Stedin Network generated in the RTDS-RSCAD environment on computer A is communicated using the IEEE standardized communication protocol, C37.118 over the TCP/IP channel. The PMU streams are further channelized to a single time-stamped data stream using a PDC. The positional time difference arises because various PMU locations are nullified and aligned at PDC. The PDC data is further communicated to computer B, where our

Table 1
The measurement accuracy for different types of measurements.

PMU measurements				Pseudo measurements
V	θ	I	δ	Power injection
3E-3%	3E-5 rad	1%	2E-1 rad	20%

Table 2
The thresholds settings for Method 1 and Method 2.

Method	Threshold values		
	γ	ζ	SIR_{th}
Method 1	4.5	3.2	–
Method 2	4.5	3.2	0.2

synchrophasor data acquisition platform (so-called SADF) decodes the transmitted data into human-readable format. This is further utilized to form true measurements for real-time SE.

4.2. Measurement and process noise covariance matrix

For simplicity reasons, the measurement error covariance matrix $\boldsymbol{R}_k$ is assumed to be diagonal. The diagonal elements of $\boldsymbol{R}_k$ represent measurement variances. Standard deviation $\boldsymbol{\sigma}(i)$ for pseudo measurements of power injections and PMU measurements of voltage and current magnitudes can be assessed as [41]:

$$\boldsymbol{\sigma}_k(i) = \frac{\text{acc}_i\,[\%]}{100} \cdot \frac{\boldsymbol{z}_k^t(i)}{3} + k_f \cdot \boldsymbol{f}(i) \tag{16}$$

where $\boldsymbol{z}^t$ is a true measurement vector; acc[%] is a measurement accuracy in percentage; k_f is a scaling coefficient; $\boldsymbol{f}$ is a meter full-scale. By considering that the accuracy of PMU voltage and current angle measurements is defined in radians, i.e. acc[rad], the standard deviation for these measurements is assessed as:

$$\boldsymbol{\sigma}_k(i) = \text{acc}_i\,[rad]/3 \tag{17}$$

Table 1 shows the measurement uncertainty for each measurement type. Here V, and θ denote bus voltage magnitude and voltage angle, respectively; I and δ denote branch current magnitude and current angle, respectively.

The process noise covariance matrix $\boldsymbol{Q}_k$ is assumed to be constant with diagonal terms all equal to 1×10^{-11}. This setting is chosen because it results in optimal estimates in quasi-steady state mode based on large number of offline simulations. The optimal value of $\boldsymbol{Q}_k$ for quasi-steady state is very small since PMU measurement uncertainties are very low [25].

4.3. Threshold settings for the adopted ADDI methods

To set the detection threshold γ, we start with the assumption that measurement NIs closely follow the Gaussian distribution. The distribution of NIs is influenced by: (a) the distribution of both process and measurement noise; (b) the linearity/non-linearity of the process model (1) and measurement model (2); (c) the settings of matrices $\boldsymbol{Q}$ and $\boldsymbol{R}$; and (d) $\boldsymbol{Q}/\boldsymbol{R}$ ratio [41]. If the process and the measurement noise follow Gaussian distribution, if (1) and (2) are linear, if $\boldsymbol{Q}$ and $\boldsymbol{R}$ correspond to their true values, and if $\boldsymbol{Q}/\boldsymbol{R}$ is small enough, it can be expected that NIs follow standard Gaussian distribution. Ideally, this means that in the absence of anomalies absolute values on NIs will be lower than 3 with 99.7% probability. However, non-linearity in (1) and/or (2), as well as approximate knowledge of $\boldsymbol{Q}$ and $\boldsymbol{R}$, can make the distribution of NIs deviate slightly from the standard Gaussian, even when the measurement noise is Gaussian distributed. The disparity is also being contributed by the process noise distribution which could also deviate from the Gaussian in the real-world applications. Consequently, the value of detection threshold γ may be different than 3

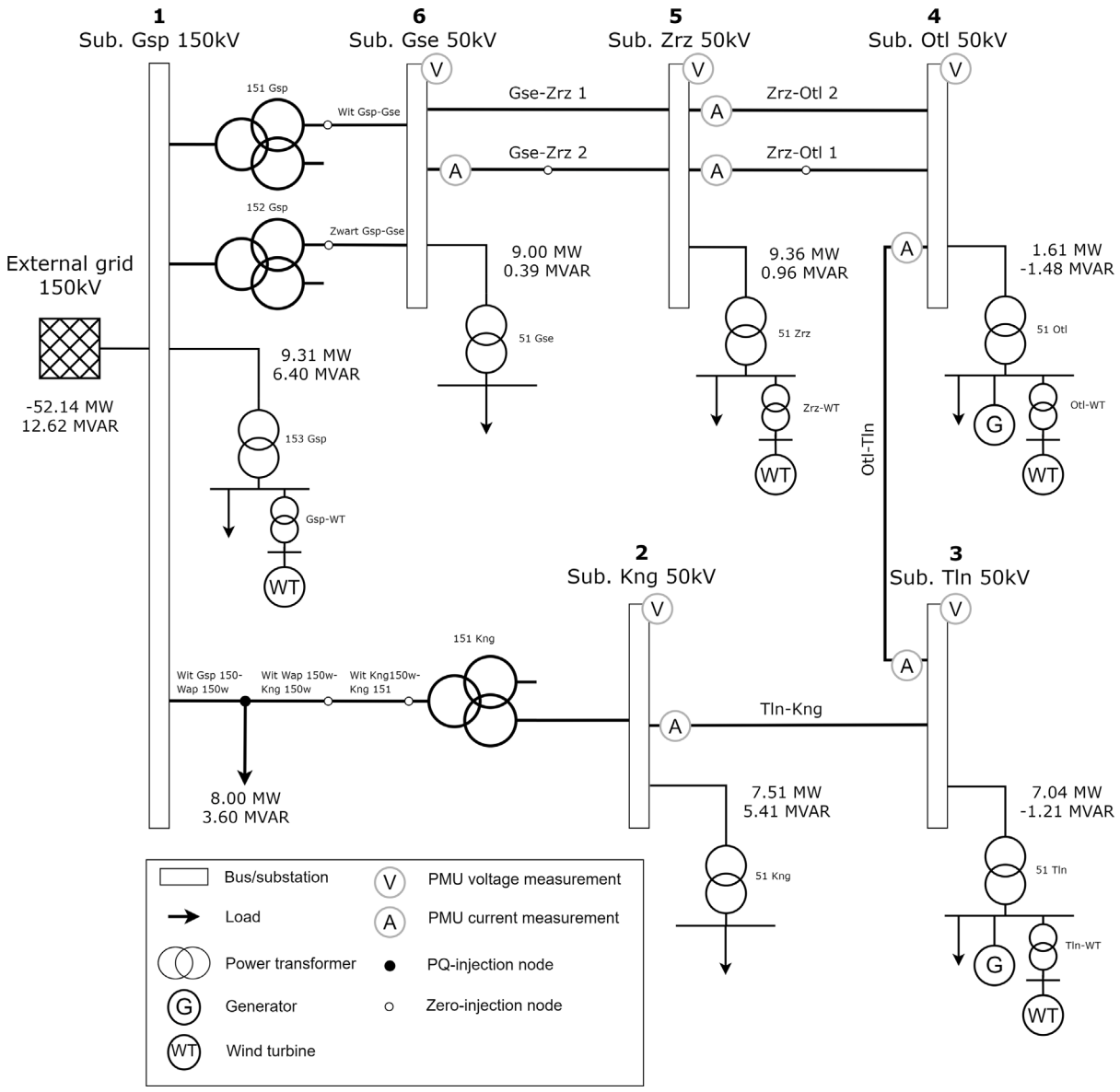

Fig. 3. An illustration of the Stedin MV grid and the PMU measurement configurations.

(usually slightly higher than 3 if $\boldsymbol{Q/R}$ is small enough). Thus, γ can be reliably established only through simulations of normal operations for each particular test system and measurement configuration. The threshold should be selected in a way to ensure that the anomalies will not be detected wrongly in their absence. In our case, extensive simulations have shown that γ =4.5 is a suitable setting if measurement noise has a Gaussian distribution.

The discrimination threshold ζ for the skewness of NIs distribution depends on the topology and measurement configuration of the network [39]. However, it is also influenced by the asymmetry level of system noise distributions. The threshold is set based on the simulations of a large number of different anomaly scenarios [14]. According to the extensive test simulation cases, the value of $\zeta = 3.2$ is selected.

Discrimination threshold SIR_{th} is selected from the condition $\mathrm{SIR}_{th} = \min(1/3, 3\sigma_{max})$ [3]. Due to the fact that σ_{max} in our system is 0.2/3 (accuracy of current angle measurements is 0.2 rad, see Table 1), the threshold is adopted to $\mathrm{SIR}_{th} = 0.2$.

Considering Gaussian measurement noise, the threshold settings for both ADDI methods are summarized in Table 2.

4.4. Performance indices

The state estimation error is assessed using (18) and (19):

$$MAE_k = \frac{1}{\mathrm{n}} \sum_{i=1}^{n} \left| \boldsymbol{x}_k^+(i) - \boldsymbol{x}_k^t(i) \right| \cdot 100 \tag{18}$$

$$MAE_i = \frac{1}{T} \sum_{k=1}^{T} \left| \boldsymbol{x}_k^+(i) - \boldsymbol{x}_k^t(i) \right| \cdot 100 \tag{19}$$

Here, MAE_k is the mean absolute error at the time sample k; $\boldsymbol{x}^t$ is the true state vector; MAE_i is the mean absolute error of the state variable i over the number of time samples T. All of the error units are either in % or crad (0.01 rad) for V and θ states, respectively.

5. Simulation results and discussions

This Section presents the real-time experimental results. The results are provided for three different operating conditions: quasi-steady state, SLC and single/multiple BD. The performance of utilized EKF FASE is compared against UKF FASE [39]. Comparison has been made

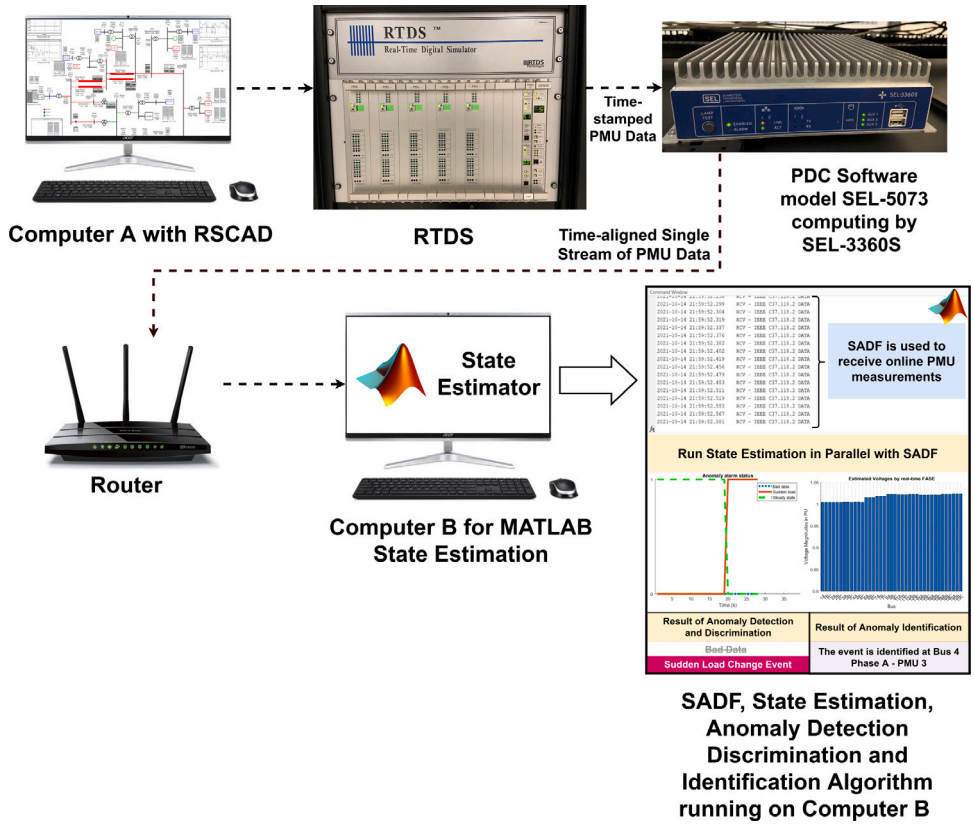

Fig. 4. Work bench description of real-time state estimator.

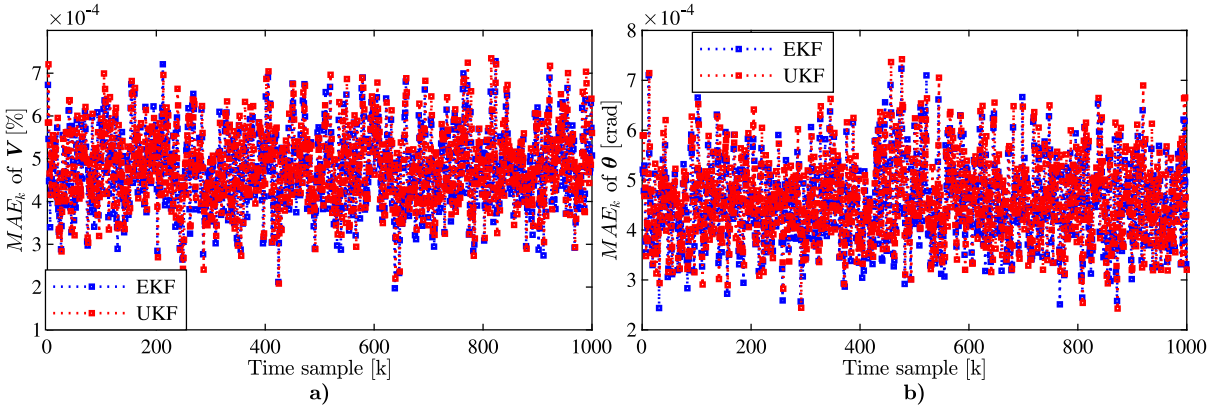

Fig. 5. MAE_k of estimated (a) voltage magnitudes and (b) voltage angles under quasi-steady state operation.

in terms of estimation accuracy, computational efficiency and compatibility with ADDI algorithm. In case of UKF, ADDI makes use of the same threshold settings like in the case of EKF (Table 2). UKF equations are provided in Appendix A. Firstly, we discuss the performance under Gaussian noise. Thereafter, the impact of non-Gaussian noise is also studied.

5.1. Quasi-steady state operation

Figs. 5 and 6 show the estimation errors MAE_k and MAE_i, respectively, obtained under quasi-steady state operation over a thousand time samples simulation period. Performance indices in Figs. 5 and 6 testify that very accurate state estimates can be achieved for both voltage magnitudes and voltage angles during quasi-steady state operation. The results indicate there is no pertinent difference in estimation accuracy between EKF and UKF.

5.2. Unpredictable sudden load changes

The findings summarized in Table 3 show that, regardless of the Kalman filter type, both Method 1 and Method 2 are able to detect, discriminate and identify SLC precisely at the moment of its occurrence. SLC scenarios are simulated at different locations and for different intensities (20%, 50% or 100% curtailment of load demand or output power of wind turbine (WT) attached to the bus). For all simulated scenarios, LNI is higher than the adopted detection threshold ($\gamma = 4.5$) enabling reliable detection either for EKF or UKF. It can be also seen that all of the skewness and the SIR values are below the adopted discrimination thresholds ($\zeta = 3.2$ and $\text{SIR}_{th} = 0.2$). Hence, Method 1 and Method 2 can discriminate anomaly as SLC reliably regardless of Kalman filter type. In addition, the identification stage can identify the PMU nearest to the SLC event by finding the measurement associated with LNI.

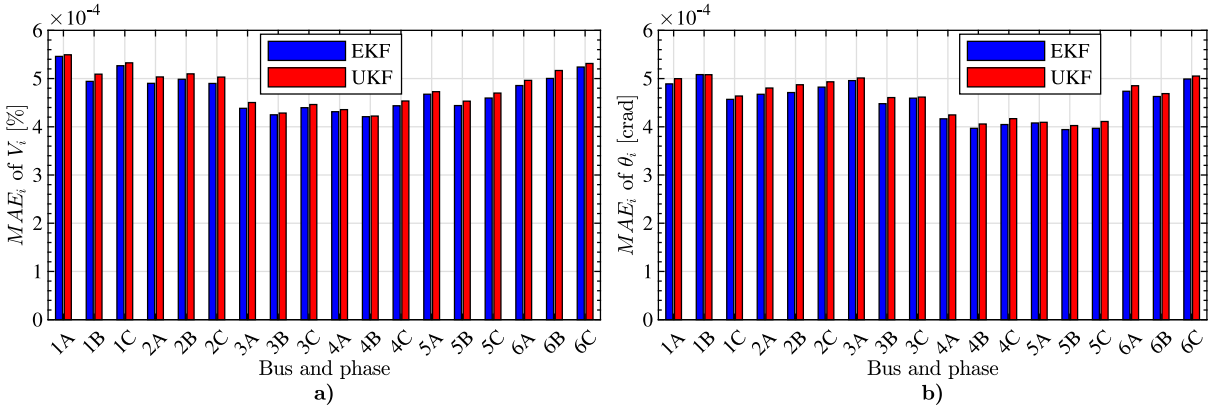

Fig. 6. MAE_i of estimated (a) voltage magnitudes and (b) voltage angles under quasi-steady state operation.

Table 3
Results of detection, discrimination and identification of SLC event.

Bus	Rated power	Intensity	LNI		Meas. with LNI		Skewness		SIR		Method 1		Method 2	
			EKF	UKF	EKF	UKF	EKF	UKF	EKF	UKF	EKF	UKF	EKF	UKF
2	Load 7.5 MW	20%	12.6	18.1	θ_{2B}	θ_{2A}	2.49	2.69	0.02	0.01	✓	✓	✓	✓
		50%	24.7	32.6	θ_{2A}	θ_{2B}	2.54	2.43	0.01	0.01	✓	✓	✓	✓
		100%	26.8	48.6	θ_{2A}	θ_{2A}	2.63	2.52	0.00	0.00	✓	✓	✓	✓
3	Load 13 MW	20%	26.5	39.9	θ_{3A}	θ_{3C}	2.12	2.03	0.01	0.01	✓	✓	✓	✓
		50%	31.0	45.3	θ_{3B}	θ_{3B}	2.20	2.13	0.00	0.00	✓	✓	✓	✓
		100%	52.5	77.6	θ_{3A}	θ_{3C}	2.19	2.17	0.00	0.00	✓	✓	✓	✓
	WT 3 MW 0.3 MVAR	100%	149	237	θ_{3B}	θ_{3B}	1.77	1.61	0.01	0.01	✓	✓	✓	✓
5	Load 20 MW	20%	10.2	23.9	θ_{5C}	θ_{5B}	1.95	1.86	0.01	0.01	✓	✓	✓	✓
		50%	21.1	26.9	θ_{5C}	θ_{5A}	1.97	1.81	0.00	0.00	✓	✓	✓	✓
		100%	31.3	42.02	θ_{5A}	θ_{5A}	2.07	1.98	0.00	0.00	✓	✓	✓	✓
	WT 10.8 MW 4MVAR	100%	762	815	θ_{5A}	θ_{5B}	1.62	1.50	0.00	0.00	✓	✓	✓	✓

Fig. 7.a shows MAE_k of estimated voltage magnitudes obtained by EKF (UKF) with and without installed ADDI module for the case of 5 MW active power curtailment of the load attached to bus 4 at time $k = 20$. Fig. 7.b shows the same accuracy index evaluated over estimated voltage angles. Once SLC hits the system, state forecasting becomes unreliable. Since the process noise covariance matrix is kept as constant, the estimation accuracy of EKF at the instant of SLC occurrence dramatically deteriorates if no action is taken (see blue line with cross markers in Fig. 7). With the ADDI module implemented, the anomaly presence is detected, the anomaly is discriminated as SLC and proper action is taken by switching from EKF FASE to the WLS SSE. This technique significantly reduces the negative impact which SLC has on estimation accuracy (see the blue line with circle markers in Fig. 7). After the moment of SLC occurrence, LNI is still high because the process model is not able to re-track the system state immediately after SLC. Consequently, the LNI test still triggers the ADDI algorithm for a certain time after SLC occurrence. Since ADDI recognizes this anomaly as SLC, WLS SSE will be consecutively executed until the LNI value becomes lower than the detection threshold ($\gamma = 4.5$) at moment $k = 42$. From here on, the estimation algorithm again switches back to the EKF filtering and utilizes the forecasted states in the filtering stage. By replacing EKF with UKF, a similar performance can be observed in terms of estimation accuracy and ADDI triggering.

5.3. Single and multiple bad data

Several test cases considering different magnitudes of single BD are simulated for PMU measurements of the voltage magnitude and angle placed at bus 2, phase A, and PMU measurements of current magnitude and angle at branch 2–3, phase A, as shown in Table 4. The gross errors of the PMU measurements are expressed in terms of the number of measurement standard deviations σ(i). From Table 4, BD with gross errors larger than 8σ(i) can be distinguished by both Method 1 and Method 2 since the skewness of NIs distribution and the SIR values are higher than the adopted discrimination thresholds ($\zeta = 3.2$ and $\text{SIR}_{th} = 0.2$). It should be highlighted that Method 1 wrongly recognizes the two cases of BD as SLC. These are gross errors of very small magnitude 8σ(i) contained in PMU measurements of current magnitude and angle at branch 2–3, phase A. In contrast, Method 2 correctly discriminates, identifies, and counters them. This is because the skewness values of NIs distribution for these two cases were lower than the defined discrimination threshold ζ; however, the SIR values were still high enough as compared to discrimination threshold SIR_{th}. Therefore, the SIR index of Method 2 helps recognizing BD with very small magnitudes. The same ADDI performance is recorded in the case of both EKF and UKF FASE.

Simultaneous presence of gross error of $20\sigma(i)$ in voltage magnitude measurement at bus 2, phase A, and gross error of $8\sigma(i)$ in current magnitude measurement at branch 2–3, phase A, is used to test the platform against multiple BD (check Table 5 for more details). Multiple BD appears successively from $k = 37$ to $k = 46$. The performances of the EKF (UKF) without and with the installed ADDI module are compared in terms of MAE_k of estimated voltage magnitudes and angles. The results are shown in Figs. 8.a and 8.b, respectively. Without the ADDI module implemented, EKF cannot recognize erroneous measurements so they slip into the filtering stage. This increases MAE_k of estimated

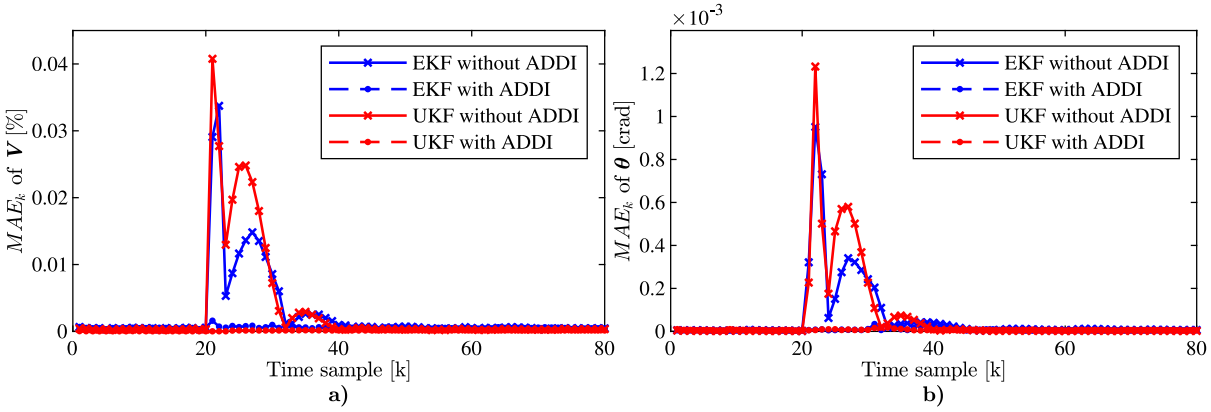

Fig. 7. MAE_k of estimated (a) voltage magnitudes and (b) voltage angles in the presence of SLC.

Table 4
Results of detection, discrimination and identification of single BD.

Measurement	BD(σ(i))	LNI		Meas. with LNI		Skewness		SIR		Method 1		Method 2	
		EKF	UKF	EKF	UKF	EKF	UKF	EKF	UKF	EKF	UKF	EKF	UKF
V_{2A}	20σ(i)	13.68	13.65	V_{2A}	V_{2A}	6.57	6.5127	0.47	0.424	✓	✓	✓	✓
V_{2A}	50σ(i)	36.3	36.26	V_{2A}	V_{2A}	9.67	9.63	0.25	0.253	✓	✓	✓	✓
δ_{2A}	20σ(i)	16.01	16.02	δ_{2A}	δ_{2A}	7.37	6.683	0.46	0.421	✓	✓	✓	✓
δ_{2A}	50σ(i)	39.83	39.74	δ_{2A}	δ_{2A}	9.61	9.703	0.24	0.244	✓	✓	✓	✓
I_{2-3A}	8σ(i)	6.78	6.77	I_{2-3A}	I_{2-3A}	2.72	2.038	0.38	0.302	✗	✗	✓	✓
I_{2-3A}	60σ(i)	56.88	56.87	I_{2-3A}	I_{2-3A}	10.44	10.118	0.18	0.178	✓	✓	✓	✓
δ_{2-3A}	8σ(i)	9.66	9.66	δ_{2-3A}	δ_{2-3A}	2.52	2.55	0.34	0.337	✗	✗	✓	✓
δ_{2-3A}	60σ(i)	58.24	58.32	δ_{2-3A}	δ_{2-3A}	9.49	9.506	0.27	0.27	✓	✓	✓	✓

Table 5
Results of detection, discrimination and identification of multiple BD.

Measurement	BD(σ(i))	$\lvert\boldsymbol{r}_k(i)\rvert$		LNI		Skewness		SIR	
		EKF	UKF	EKF	UKF	EKF	UKF	EKF	UKF
V_{2A}	20σ(i)	14.85	13.63	14.85	13.63	5.85	5.36	0.39	0.39
δ_{2-3A}	8σ(i)	6.56	6.74						

voltage magnitudes whilst the accuracy of the voltage angle estimates is less affected (voltage magnitude measurement is one of the PMUs corrupted with BD). With ADDI implemented, the system detects the presence of the anomaly using the LNI test (check Table 5). After determining the anomaly as BD based on skewness and SIR, the two erroneous measurements are correctly identified and replaced by the corresponding forecasted measurements. Next, EKF filters the noise, and provides the estimation accuracy like in normal operation. Similar considerations apply to the UKF results. It has been noticed that both Method 1 and Method 2 discriminate this case as multiple BD, even though one of the two bad measurements contains a gross error of very small magnitude. Therefore, small gross errors of 8σ(i) can be considered as a borderline case for ADDI: sometimes ADDI will be able to discriminate it properly, however sometimes not. It is expected that gross errors smaller than 8σ(i) cannot be discriminated correctly using ADDI. Anyway, these BD are of very small intensity and even if they slip into the filtering stage as a single bad measurement they are not powerful enough to deteriorate estimation accuracy.

5.4. Impact of non-Gaussian measurement noise

Although measurement noise is routinely considered with a Gaussian distribution [46], certain works report that measurement noise of realistic PMUs is unlikely to follow Gaussian distribution [47,48]. If the Gaussian assumption is violated, the setting of the detection threshold γ provided in Table 2 should be revised. To analyze the impact of a non-Gaussian measurement noise, we consider two more cases: when measurement noise makes use of Laplacian distribution and when it follows the Gaussian mixture (GM) distribution of two Gaussian components. In the first case, the Laplacian distribution of the ith measurement has a zero mean and a scale parameter $\sigma(i)$. In case of GM distribution, noise components of the ith measurement are represented with mean values of $0.5\sigma(i)$ and $2\sigma(i)$, with standard deviations of $0.7\sigma(i)$ and $1.3\sigma(i)$, and with weights of 0.7 and 0.3, respectively. The parameters for Laplace and GM distribution can be found in [49], whilst the probability density functions of these distributions are given in Appendix B.

Fig. 9 shows LNI values obtained during quasi-steady state operation considering different distributions for the measurement noise. This has been done for both EKF and UKF FASE. In the case of Gaussian measurement noise, it can be seen that LNI picks up the value higher than 3 not so rarely. As discussed in Section 4.3, this is due to system nonlinearities and limited knowledge about system noise statistics ($\boldsymbol{Q}$ and $\boldsymbol{R}$), because of which NIs follow Gaussian distribution only approximately (despite the measurement noise is ideally Gaussian). To ensure LNI values will not trigger ADDI during normal operation, the detection threshold is set to $\gamma = 4.5$. In this way, LNI values stay lower than the threshold γ during the whole simulation period if the measurement noise is Gaussian distributed. However, in the case of non-Gaussian noise, LNI occasionally exceeds this detection threshold. This is expected since both Laplace and GM measurement noise with assumed distribution parameters have longer tails as compared to the Gaussian measurement noise (check Fig. B.1 in Appendix B). Longer tails in measurement noise reflect an increase in NIs, as a result of which threshold γ needs to be readjusted. The new setting depends on the properties of measurement noise. In the case of a Laplacian

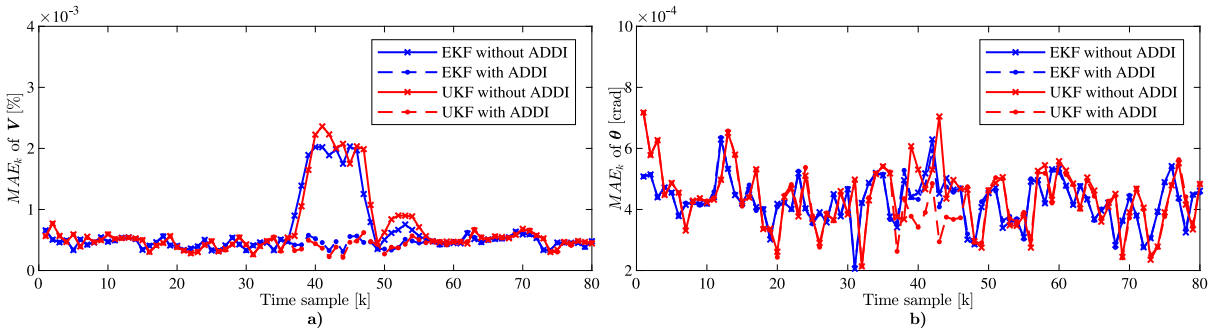

Fig. 8. MAE_k of estimated (a) voltage magnitudes and (b) voltage angles in the presence of multiple BD.

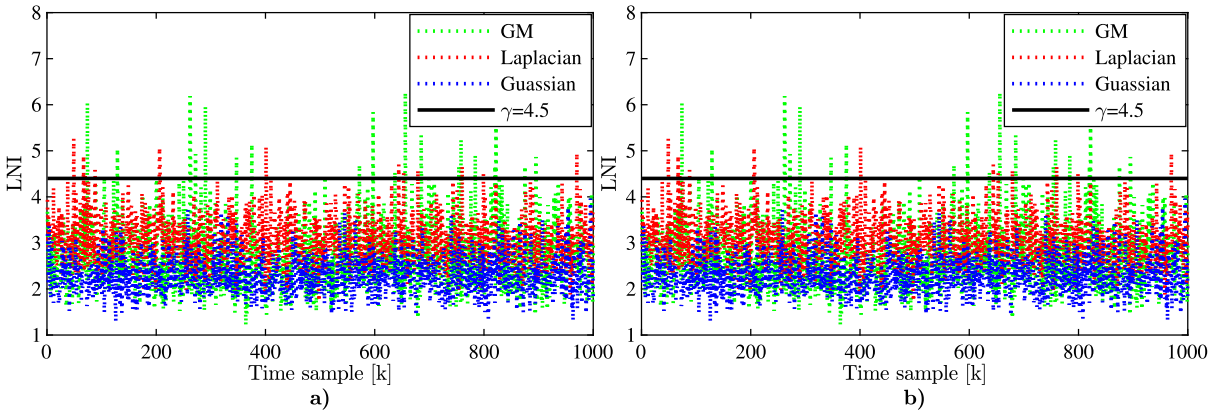

Fig. 9. LNI during quasi-steady state operation considering different measurement noise distributions in case of (a) EKF and (b) UKF FASE.

measurement noise with assumed distribution parameters, it can be expected that during normal operation LNI should be lower than 5.8 with a probability of 99.7% (ideally). Again, due to system nonlinearities and only approximate knowledge of $\boldsymbol{Q}$ and $\boldsymbol{R}$, LNI might be slightly higher than 5.8. After simulations were run, it turned out that γ=6.5 can be used as a detection threshold in the case of Laplace measurement noise. Similar considerations can be applied in the case of GM measurement noise for which γ=7 enables reliable detection. Comparing Figs. 9.a and 9.b, it can be seen that the choice of Kalman filter type does not affect conclusions regarding γ readjustment.

To analyze how non-Gaussian measurement noise impacts selection of discrimination thresholds ζ and SIR_{th}, extensive simulations of abnormal operating conditions have been conducted considering the assumption that measurement noise under normal operation is distributed according to Laplace or GM distribution. Due to lack of space, Fig. 10 shows the results for only a few of simulated anomalies: small BD appears from time k = 146 to k = 176, this is followed by a large SLC case at k = 500, and lastly a large BD is introduced from k = 800 to k = 840. The rest of the simulation period system is in a normal quasi-steady state operation. As it can be seen from Fig. 10, skewness ψ and SIR are calculated only when ADDI detects the presence of an anomaly (when LNI is higher than the adopted detection threshold γ). Next, there is no significant difference in skewness ψ for different types of distributions that would require readjustment for discrimination threshold ζ = 3.2. Discrimination threshold ζ adopted based on a Gaussian assumption will be able to discriminate SLC from BD even when the measurement noise follows a Laplacian or a GM distribution. In the case of BD, skewness ψ keeps a high value regardless of measurement noise distribution (except in the case of very small BD, which will be demonstrated later). Skewness for all simulated SLC scenarios stays below the threshold ζ; since skewness is a measure of asymmetry in the distributions and since the Laplacian noise is with a symmetric distribution, the skewness of NIs in case of a Laplacian measurement noise stays the same as in the case of Gaussian measurement noise. On the other hand, slightly higher skewness values are recorded under SLC for a GM measurement noise since GM distribution is not symmetrical. For the assumed parameters of the GM distribution, it turned out that the asymmetry level is not crucially large to make the skewness exceeding the adopted threshold ζ = 3.2, thus not requiring any readjustment of the threshold ζ. Yet, it should be highlighted that for some distributions with higher asymmetry levels this might not be the case, so the discrimination threshold ζ should be readjusted accordingly. Therefore, it is always necessary to revise the setting for ζ through the simulations. Similar conclusions can be withdrawn for discrimination threshold SIR_{th}. Again, replacing EKF with UKF will not change conclusions about the impact of non-Gaussian measurement noise on discrimination thresholds ζ and SIR_{th}.

To verify the performance of Method 1 and Method 2 after the readjustment of ADDI thresholds, simulations are repeated by selecting new random SLC and BD scenarios: a single small BD of $8\sigma(i)$ and $10\sigma(i)$ appears from time sample k = 146 to k = 176 and k = 200 to 240, respectively; thereafter, a large SLC happens at k = 500, and finally, a large BD case of $60\sigma(i)$ occurs from k = 800 to k = 840. The rest of the time system operates in a normal quasi-steady state (QSS). Due to lack of space, in Fig. 11 results have been shown only for the case of Laplacian measurement noise and EKF FASE. The new set of threshold settings for the Laplacian noise are: γ = 6.5, ζ = 3.2 and SIR_{th} = 0.2. If BD of 8σ appears this time, ADDI not only fails to discriminate the anomaly as BD (as that was the case when the measurement noise was with a Gaussian distribution) but it also fails to detect the anomaly presence. This is expected because longer tails of Laplacian measurements noise require a new setting for threshold γ to be 6.5, which is very close to 8. This makes it very hard for the LNI test to clearly separate a normal operation from such a small BD. To check when the LNI test becomes able to clearly detect the presence of small BD, small BD is increased to $10\sigma(i)$. As it can be seen from Fig. 11, the presence of this anomaly is detected for all time samples between

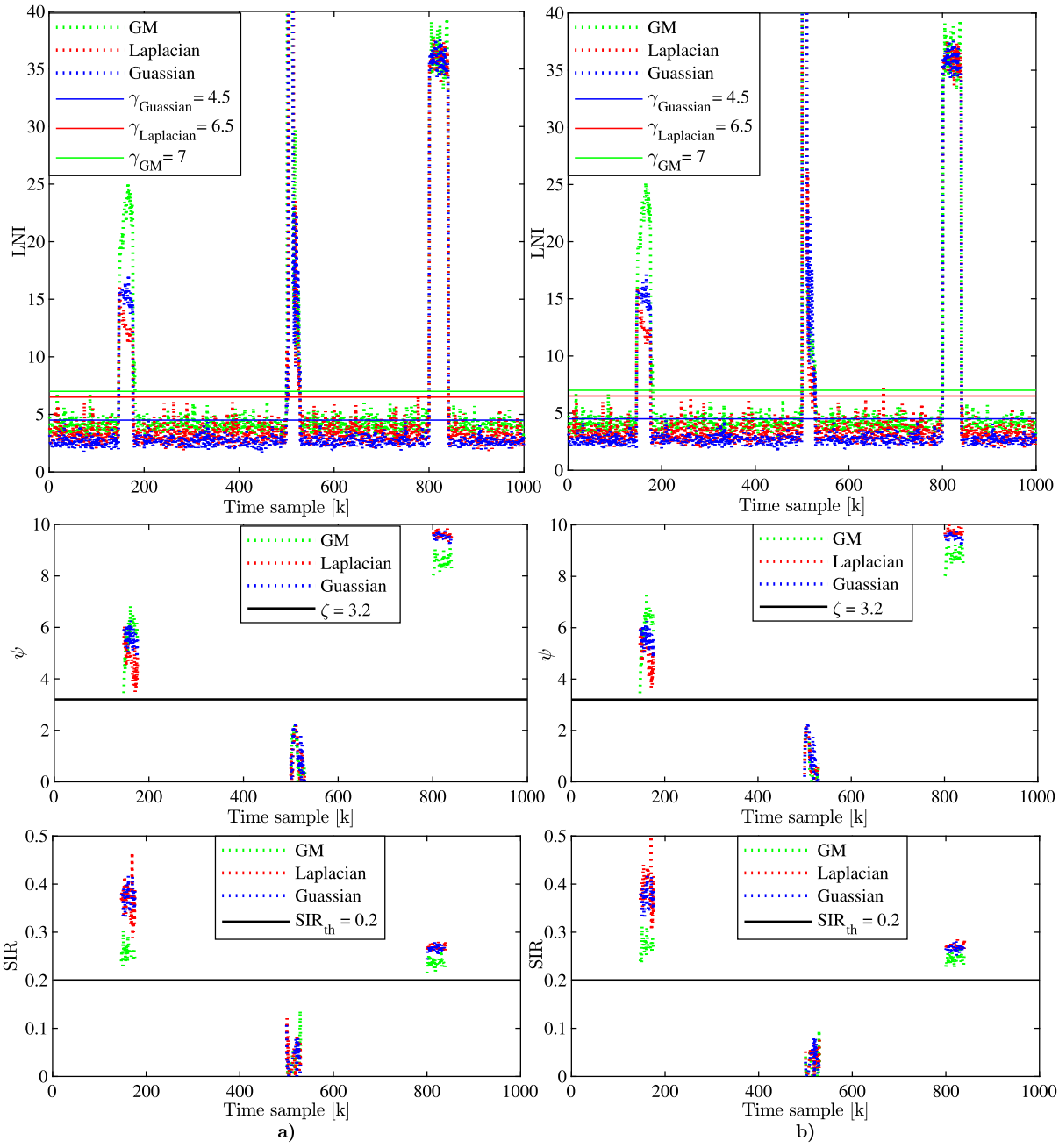

Fig. 10. Detection and discrimination thresholds during normal and abnormal operation considering different measurement noise distributions in case of (a) EKF and (b) UKF FASE.

$k = 200$ and $k = 240$. However, within this time interval, the skewness varies around the discrimination threshold ψ aggravating Method 1 to discriminate the anomaly correctly. Still, Method 2 discriminates the anomaly as BD without any problem by utilizing the SIR index. SIR keeps its value above the discrimination threshold at all times between $k = 200$ and $k = 240$. On the other hand, large SLC and large BD are detected and discriminated properly by both Method 1 and Method 2. Therefore, the verification results prove that with new settings for non-Gaussian measurement noise, both Method 1 and Method 2 can provide the same performance as in the case of a Gaussian noise with corresponding thresholds applied.

5.5. Computational time

In this work, the distribution network and the measurement devices are modeled in RTDS-RSCAD. The PMUs simulated by the RTDS has been set to a refresh rate of 50 Hz (20 ms). In general, there are two types of latencies: the time taken by the data communication system to send the PMU signals from the RTDS to Computer B, and the computational time of the SE algorithm including ADDI [50]. Overall, the average time to read a single PMU data in a Matlab environment after being triggered in the RTDS environment will be 0.31 ms to 0.78 ms [51]. This time includes telecommunication and PDC latencies. On the other hand, the computational time required to perform SE depends on the hardware and the type of the SE algorithm. The Computer B specification is already mentioned in Section 4. EKF algorithm approximates the nonlinear measurement model by calculating first-order partial derivatives at the point of linearization. UKF utilizes unscented transformation based on the propagation of chosen sigma points (this way calculation of the Jacobian matrix is avoided).

The average computational time of the EKF and the UKF FASE coupled with the ADDI algorithm is shown in Table 6 for different

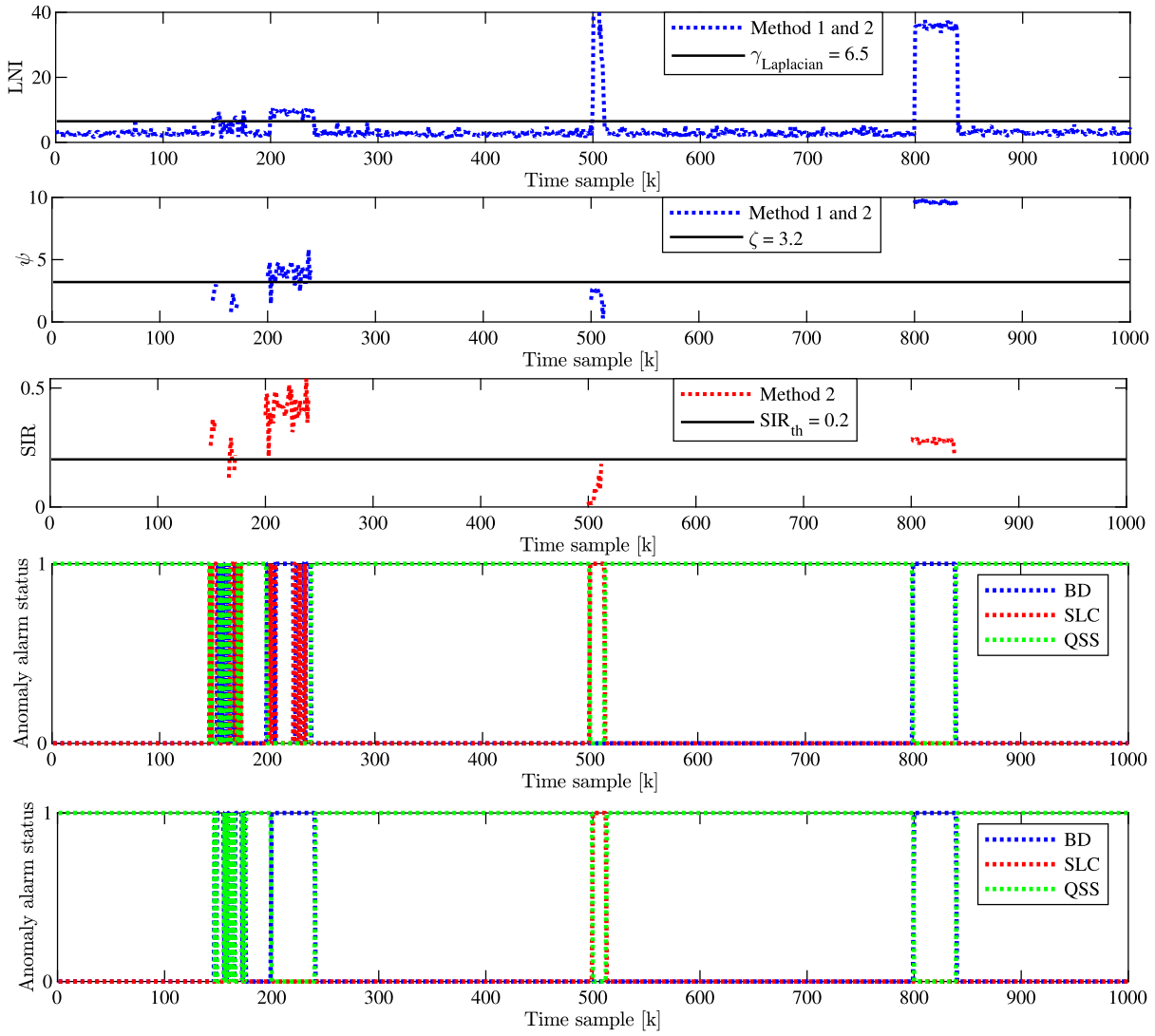

Fig. 11. Performance verification of ADDI Method 1 and Method 2 in EKF FASE framework considering Laplacian distributed measurement noise.

operation conditions. The computational time starts from the instant of receiving the PMU measurements until the instant when final estimates are obtained. The findings reveal that the average execution time per one-time sample is lower for EKF than for UKF regardless of the operating conditions. Considering that the measurement vector is composed mostly of linear PMU measurements, only a few of the first derivatives are computed when new measurements arrive, whilst most of them remain unchanged. In case of UKF, each sigma point has to be propagated through both process and measurement models, which obviously results in a higher computational time for UKF as compared to EKF.

The computational times reported in Table 6 indicate that EKF is more suitable for the real-time state estimation platform since it is capable to follow the high-speed refresh rate of PMUs under not only normal but also abnormal operation. Slightly higher computational time in the presence of anomalies follows from the fact that ADDI excecutes discrimination and identification after the detection stage is done. During normal operation, the ADDI role ends up after the detection stage is executed (since there is no anomaly in the system). This results in lower computational time as compared to the case when an anomaly occurs.

Table 6
Average computational time under three different operating conditions.

Qausi-steady state		Sudden load change		Bad data	
EKF	UKF	EKF	UKF	EKF	UKF
13.7 ms	40.1 ms	24.1 ms	52.3 ms	18.5 ms	43.6 ms

6. Conclusion

In this paper, real-time Distribution System State Estimation platform based on PMUs is developed and demonstrated. The platform is tested and validated using Real Time Digital Simulator in order to evaluate the possibility of implementation into the actual 50 kV ring of a Stedin network located in the southwest (Zeeland area) of the Netherland. First emulated results indicate that real-time Distribution System State Estimation might be feasible when proper state estimation methods for data processing are used.

To provide high computational efficiency necessary to catch up with the fast refresh rates of PMUs, the FASE algorithm based on the EKF has been implemented into the platform. The advantages of FASE are used to achieve fast and reliable ADDI that can meet the high-efficient computational requirements. Two ADDI methods are tested considering different probability distributions of the measurement noise. Extensive

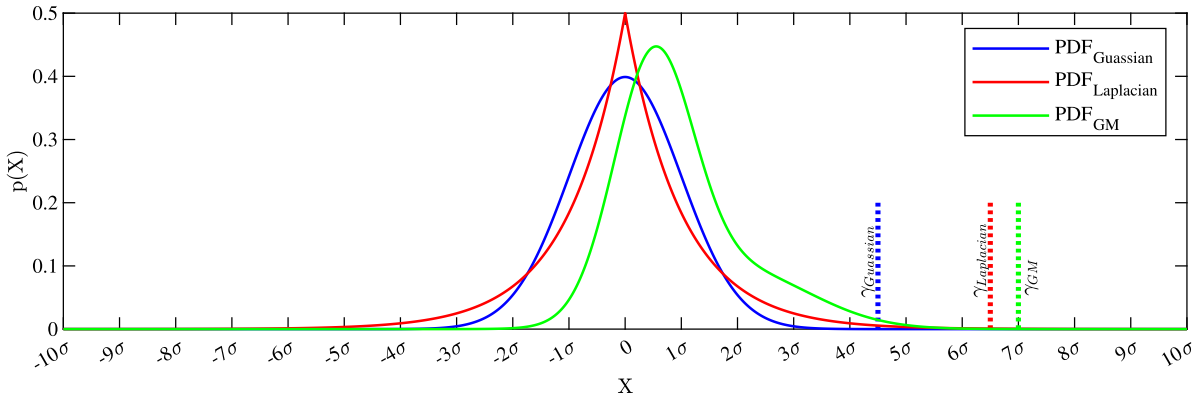

Fig. B.1. Probability density functions (PDFs) of Gaussian, Laplacian and Gaussian Mixture noises along with the corresponding detection thresholds.

simulations have shown that different noise statistics require different threshold settings for ADDI methods. However, type of noise generally does not affect the performance of the ADDI methods if the threshold settings are chosen properly according to that type of noise..

To check its eligibility for a real-time state estimation platform, EKF has been compared to another Kalman filter extension for nonlinear systems — UKF. EKF and UKF provide similar estimation accuracy and compatibility with ADDI methods under various operating conditions. Yet, EKF is computationally more efficient and thus more suitable for real-time applications. Although ADDI proves to be computationally efficient and accurate against BD and SLC, it is necessary to further investigate its capabilities against more challenging anomalies like malicious data attacks and topology changes. The main challenge is how to extend ADDI to cope with these anomalies without losing the computational efficiency necessary for PMU-based real-time state estimation. Our future work will try to address these issues, as well as how to utilize the developed platform for a fault location at a later stage.

Declaration of competing interest

The authors declare that they have no known competing financial interests or personal relationships that could have appeared to influence the work reported in this paper.

Data availability

The data that has been used is confidential.

Acknowledgments

The research work was jointly supported by the Dutch Scientific Council NWO in collaboration with TSO TenneT, DSOs Alliander, Stedin, VSL and General Electric in the framework of the Energy System Integration & Big Data program under the project “Resilient Synchromeasurement-based Grid Protection Platform, no. 647.003.004”. Additionally, the work is supported by the Engineering and Physical Sciences Research Council (EPSRC) of UK (Grant No. EP/S00078X/2 and Grant No. EP/T021969/1), and the Ministry of Education, Science and Technological Development of the Republic of Serbia (Grant No. 451-03-68/2022-14/200132 with University of Kragujevac - Faculty of Technical Sciences Čačak).

Appendix A

UKF-based FASE utilizes the following set of equations [42]:

$$\boldsymbol{Y}_k^+ = \boldsymbol{x}_k^+ \cdot \mathbf{1}^T + \sqrt{\mathrm{n}+\lambda}\begin{bmatrix}\mathbf{0} & \sqrt{\boldsymbol{P}_k^+} & -\sqrt{\boldsymbol{P}_k^+}\end{bmatrix} \tag{A.1}$$

$$\boldsymbol{X}_{k+1}^- = \boldsymbol{F}_k \boldsymbol{Y}_k^+ + \boldsymbol{g}_k \cdot \mathbf{1}^T \tag{A.2}$$

$$\boldsymbol{x}_{k+1}^- = \boldsymbol{X}_{k+1}^- \boldsymbol{w}_{\mathrm{m}} \tag{A.3}$$

$$\boldsymbol{P}_{k+1}^- = \boldsymbol{X}_{k+1}^- \boldsymbol{W} \left[\boldsymbol{X}_{k+1}^-\right]^{\mathrm{T}} + \boldsymbol{Q}_k \tag{A.4}$$

$$\boldsymbol{Y}_{k+1}^- = \boldsymbol{x}_{k+1}^- \cdot \mathbf{1}^T + \sqrt{\mathrm{n}+\lambda}\begin{bmatrix}0 & \sqrt{\boldsymbol{P}_{k+1}^-} & -\sqrt{\boldsymbol{P}_{k+1}^-}\end{bmatrix} \tag{A.5}$$

$$\boldsymbol{Z}_{k+1}^- = h\left(\boldsymbol{Y}_{k+1}^-\right) \tag{A.6}$$

$$\boldsymbol{\nu}_{k+1} = \boldsymbol{z}_{\boldsymbol{k+1}} - \boldsymbol{Z}_{\boldsymbol{k+1}}^- \boldsymbol{w}_{\mathrm{m}} \tag{A.7}$$

$$\boldsymbol{S}_{k+1} = \boldsymbol{Z}_{k+1}^- \boldsymbol{W} \left[\boldsymbol{Z}_{k+1}^-\right]^T + \boldsymbol{R}_{k+1} \tag{A.8}$$

$$\boldsymbol{C}_{k+1} = \boldsymbol{Y}_{k+1}^- \boldsymbol{W} \left[\boldsymbol{Z}_{k+1}^-\right]^T \tag{A.9}$$

$$\boldsymbol{K}_{k+1} = \boldsymbol{C}_{k+1} \boldsymbol{S}_{k+1}^{-1} \tag{A.10}$$

$$\boldsymbol{x}_{k+1}^+ = \boldsymbol{x}_{k+1}^- + \boldsymbol{K}_{k+1} \boldsymbol{\nu}_{k+1} \tag{A.11}$$

$$\boldsymbol{P}_{k+1}^+ = \boldsymbol{P}_{\boldsymbol{k+1}}^- - \boldsymbol{K}_{k+1} \boldsymbol{S}_{k+1} \boldsymbol{K}_{k+1}^T \tag{A.12}$$

where $\boldsymbol{Y}^+$ is $\mathrm{n}\times(2\mathrm{n}+1)$ matrix of sigma points corresponding to the estimated state vector $\boldsymbol{x}^+$ (each column in $\boldsymbol{Y}^+$ represents one sigma point); λ is scaling parameter; $\mathbf{1}$ is $(2\mathrm{n}+1)\times 1$ vector of all ones; $\mathbf{0}$ is $\mathrm{n}\times 1$ zero vector; $\boldsymbol{X}^-$ is $\mathrm{n}\times(2\mathrm{n}+1)$ matrix made up of sigma points propagated through process model (1); $\boldsymbol{w}_m$ and $\boldsymbol{W}$ are $(2\mathrm{n}+1)\times 1$ weight vector and $(2\mathrm{n}+1)\times(2\mathrm{n}+1)$ weighting matrix, respectively; $\boldsymbol{Y}^-$ is $\mathrm{n}\times(2\mathrm{n}+1)$ matrix of sigma points corresponding to the forecasted state vector; $\boldsymbol{Z}^-$ is $\mathrm{m}\times(2\mathrm{n}+1)$ matrix made up of sigma points propagated through measurement model (2); $\boldsymbol{C}$ is $\mathrm{n}\times\mathrm{m}$ cross-covariance matrix of the state and measurement. Scaling parameter λ and weights $\boldsymbol{w}_{\mathrm{m}}$ and $\boldsymbol{W}$ are calculated as:

$$\lambda = \alpha^2(\mathrm{n}+\kappa) - \mathrm{n} \tag{A.13}$$

$$\boldsymbol{w}_{\mathrm{m}} = \begin{bmatrix} w_{\mathrm{m}}^{(0)} & \cdots & w_{\mathrm{m}}^{(2\mathrm{n})}\end{bmatrix}^T \tag{A.14}$$

$$\boldsymbol{W} = \left(\boldsymbol{I}_{2\mathrm{n}+1} - \begin{bmatrix}\boldsymbol{w}_{\mathrm{m}} & \cdots & \boldsymbol{w}_{\mathrm{m}}\end{bmatrix}\right) \cdot diag\left\{w_c^{(0)} \quad \cdots \quad w_c^{(2\mathrm{n})}\right\} \cdot \left(\boldsymbol{I}_{2\mathrm{n}+1} - \begin{bmatrix}\boldsymbol{w}_{\mathrm{m}} & \cdots & \boldsymbol{w}_{\mathrm{m}}\end{bmatrix}\right)^T \tag{A.15}$$

where $w_{\mathrm{m}}^{(0)} = \lambda/(\mathrm{n}+\lambda)$; $w_c^{(0)} = \lambda/(\mathrm{n}+\lambda) + (1-\alpha^2+\beta)$; $w_{\mathrm{m}}^{(j)} = w_c^{(j)} = 1/\{2(\mathrm{n}+\lambda)\}, j = 1, \ldots, 2\mathrm{n}$; $\boldsymbol{I}_{2\mathrm{n}+1}$ is $(2\mathrm{n}+1)\times(2\mathrm{n}+1)$ identity matrix; α, β and κ are UKF parameters set as $\alpha = 1$, $\beta = 2$ and $\kappa = 3 - \mathrm{n}$.

Appendix B

Probability density function p(X) of a random variable X is shown in Fig. B.1 for three different probability distributions used in this paper: Gaussian, Laplacian, and Gaussian Mixture.

References

[1] Schweppe FC, Wildes J. Power System static-state estimation, Part I: Exact model. IEEE Trans Power Appar Syst 1970;PAS-89(1):120–5. http://dx.doi.org/10.1109/TPAS.1970.292678.

[2] Schweppe FC. Power system static-state estimation, Part III: Implementation. IEEE Trans Power Appar Syst 1970;PAS-89(1). http://dx.doi.org/10.1109/TPAS.1970.292680.

[3] Jin Z, Chakrabarti S, Yu J, Ding L, Terzija V. An improved algorithm for cubature Kalman filter based forecasting-aided state estimation and anomaly detection. Int Trans Electr Energy Syst 2021;31(5):e12714. http://dx.doi.org/10.1002/2050-7038.12714.

[4] Carquex C, Rosenberg C, Bhattacharya K. State estimation in power distribution systems based on ensemble Kalman filtering. IEEE Trans Power Syst 2018;33(6):6600–10. http://dx.doi.org/10.1109/TPWRS.2018.2847289.

[5] Do Coutto Filho MB, de Souza JC. Forecasting-aided state estimation—Part I: Panorama. IEEE Trans Power Syst 2009;24(4):1667–77. http://dx.doi.org/10.1109/TPWRS.2009.2030295.

[6] Zhao J, Mili L. Robust unscented Kalman filter for power system dynamic state estimation with unknown noise statistics. IEEE Trans Smart Grid 2019;10(2):1215–24. http://dx.doi.org/10.1109/TSG.2017.2761452.

[7] Zhou N, Meng D, Huang Z, Welch G. Dynamic state estimation of a synchronous machine using PMU data: A comparative study. 2015, p. 1. http://dx.doi.org/10.1109/PESGM.2015.7285966.

[8] Qi J, Taha AF, Wang J. Comparing Kalman filters and observers for power system dynamic state estimation with model uncertainty and malicious cyber attacks. IEEE Access 2018;6:77155–68. http://dx.doi.org/10.1109/ACCESS.2018.2876883.

[9] Tebianian H, Jeyasurya B. Dynamic state estimation in power systems using Kalman filters. In: 2013 IEEE electrical power & energy conference. 2013, p. 1–5. http://dx.doi.org/10.1109/EPEC.2013.6802979.

[10] Abur A, Gomez-Exposito A. Power system state estimation: Theory and implementation, Vol. 24. 2004, http://dx.doi.org/10.1201/9780203913673.

[11] Ashok A, Govindarasu M, Ajjarapu V. Online detection of stealthy false data injection attacks in power system state estimation. IEEE Trans Smart Grid 2018;9(3):1636–46. http://dx.doi.org/10.1109/TSG.2016.2596298.

[12] Lin Y, Abur A. A highly efficient bad data identification approach for very large scale power systems. IEEE Trans Power Syst 2018;33(6):5979–89. http://dx.doi.org/10.1109/TPWRS.2018.2826980.

[13] Li WT, Wen CK, Chen JC, Wong KK, Teng JH, Yuen C. Location identification of power line outages using PMU measurements with bad data. IEEE Trans Power Syst 2016;31(5):3624–35. http://dx.doi.org/10.1109/TPWRS.2015.2495214.

[14] Nishiya K, Hasegawa J, Koike T. Dynamic state estimation including anomaly detection and identification for power systems. IEEE Proc C (Gener, Transm Distrib) 1982;129(5):192–8.

[15] da Silva AML, Do Coutto Filho MB, Cantera JMC. An Efficient Dynamic State Estimation Algorithm including Bad Data Processing. IEEE Trans Power Syst 1987;2(4):1050–8. http://dx.doi.org/10.1109/TPWRS.1987.4335300.

[16] Do Coutto Filho MB, da Silva AML, Cantera JMCC, da Silva RA. Information debugging for real-time power systems monitoring. IEE Proc C (Gener, Transm Distrib) 1989;136(3):145–52.

[17] Singh D, Pandey JP, Chauhan DS. Topology identification, bad data processing, and state estimation using fuzzy pattern matching. IEEE Trans Power Syst 2005;20(3):1570–9. http://dx.doi.org/10.1109/TPWRS.2005.852086.

[18] Lefebvre S, Prévost J. Topology error detection and identification in network analysis. Int J Electr Power Energy Syst 2006;28(5):293–305. http://dx.doi.org/10.1016/J.IJEPES.2005.12.006.

[19] Jin Z, Zhao J, Ding L, Chakrabarti S, Gryazina E, Terzija V. Power system anomaly detection using innovation reduction properties of iterated extended Kalman filter. Int J Electr Power Energy Syst 2022;136:107613. http://dx.doi.org/10.1016/J.IJEPES.2021.107613.

[20] Weng Y, Ilić MD, Li Q, Negi R. Distributed algorithms for convexified bad data and topology error detection and identification problems. Int J Electr Power Energy Syst 2016;83:241–50. http://dx.doi.org/10.1016/J.IJEPES.2016.03.044.

[21] Monticelli A. Electric power system state estimation. Proc IEEE 2000;88(2):262–82. http://dx.doi.org/10.1109/5.824004.

[22] Sexauer J, Javanbakht P, Mohagheghi S. Phasor measurement units for the distribution grid: Necessity and benefits. In: 2013 IEEE PES innovative smart grid technologies conference. 2013, http://dx.doi.org/10.1109/ISGT.2013.6497828.

[23] Bolognani S, Carli R, Todescato M. State estimation in power distribution networks with poorly synchronized measurements. In: Proceedings of the IEEE conference on decision and control, Vol. 2015-February, no. February. Institute of Electrical and Electronics Engineers Inc.; 2014, p. 2579–84. http://dx.doi.org/10.1109/CDC.2014.7039783.

[24] Von Meier A, Culler D, McEachern A, Arghandeh R. Micro-synchrophasors for distribution systems. In: 2014 IEEE PES innovative smart grid technologies conference. IEEE Computer Society; 2014, http://dx.doi.org/10.1109/ISGT.2014.6816509.

[25] Zanni L, Sarri S, Pignati M, Cherkaoui R, Paolone M. Probabilistic assessment of the process-noise covariance matrix of discrete Kalman filter state estimation of active distribution networks. In: 2014 International conference on probabilistic methods applied to power systems, PMAPS 2014 - conference proceedings. Institute of Electrical and Electronics Engineers Inc.; 2014, http://dx.doi.org/10.1109/PMAPS.2014.6960646.

[26] Sarri S, Paolone M, Cherkaoui R, Borghetti A, Napolitano F, Nucci CA. State estimation of active distribution networks: Comparison between WLS and iterated Kalman-filter algorithm integrating PMUs. In: IEEE PES innovative smart grid technologies conference Europe. 2012, http://dx.doi.org/10.1109/ISGTEUROPE.2012.6465871.

[27] Zhang L, Lai K. A novel complex linear state estimator for smart power distribution systems: Methodology and implementation. Int J Electr Power Energy Syst 2020;123:106312. http://dx.doi.org/10.1016/J.IJEPES.2020.106312.

[28] Muscas C, Pau M, Pegoraro PA, Sulis S. Uncertainty of voltage profile in PMU-based distribution system state estimation. IEEE Trans Instrum Meas 2016;65(5):988–98. http://dx.doi.org/10.1109/TIM.2015.2494619.

[29] De Oliveira-De Jesus PM, Rodriguez NA, Celeita DF, Ramos GA. PMU-based system state estimation for multigrounded distribution systems. IEEE Trans Power Syst 2021;36(2):1071–81. http://dx.doi.org/10.1109/TPWRS.2020.3017543.

[30] Gholami M, Tehrani Fard AA, Moeini-Aghtaie M. Linear voltage based state estimator for active distribution system including phasor measurement unit (PMU). In: 23rd Electrical power distribution conference. Institute of Electrical and Electronics Engineers Inc.; 2018, p. 5–10. http://dx.doi.org/10.1109/EPDC.2018.8536296.

[31] Muscas C, Pau M, Pegoraro PA, Sulis S, Ponci F, Monti A. Multiarea distribution system state estimation. IEEE Trans Instrum Meas 2015;64(5):1140–8. http://dx.doi.org/10.1109/TIM.2014.2365406.

[32] Pignati M, Popovic M, Barreto S, Cherkaoui R, Dario Flores G, Le Boudec JY, et al. Real-time state estimation of the EPFL-campus medium-voltage grid by using PMUs. In: 2015 IEEE power and energy society innovative smart grid technologies conference. Institute of Electrical and Electronics Engineers Inc.; 2015, http://dx.doi.org/10.1109/ISGT.2015.7131877.

[33] Faruque MO, Strasser T, Lauss G, Jalili-Marandi V, Forsyth P, Dufour C, et al. Real-time simulation technologies for power systems design, testing, and analysis. IEEE Power Energy Technol Syst J 2015;2:63–73. http://dx.doi.org/10.1109/JPETS.2015.2427370.

[34] Mutanen A, Repo S, Järventausta P, Löf A, Giustina DD. Testing low voltage network state estimation in RTDS environment. In: 2013 4th IEEE/PES innovative smart grid technologies Europe. 2013, http://dx.doi.org/10.1109/ISGTEurope.2013.6695482.

[35] Pulok MKH, Faruque MO. Real-Time dynamic state estimation using synchrophasor data. In: 2015 North American power symposium. NAPS 2015, Institute of Electrical and Electronics Engineers Inc.; 2015, http://dx.doi.org/10.1109/NAPS.2015.7335169.

[36] Khazraj H, Adewole AC, Annakkage UD, Faria Da Silva F, Bak CL, Rajapakse AD. Online synchrophasor-based dynamic state estimation using real-time digital simulator. In: Proceedings - 2018 IEEE international conference on environment and electrical engineering and 2018 IEEE industrial and commercial power systems Europe. Institute of Electrical and Electronics Engineers Inc.; 2018, http://dx.doi.org/10.1109/EEEIC.2018.8494221.

[37] Ali I, Huzaifa M, Ullah O, Aftab MA, Anis MZ. Real time microgrid state estimation using phasor measurement unit. In: 2019 International conference on power electronics, control and automation, ICPECA 2019 - proceedings, Vol. 2019-November. Institute of Electrical and Electronics Engineers Inc.; 2019, http://dx.doi.org/10.1109/ICPECA47973.2019.8975460.

[38] Sharma A, Srivastava SC, Chakrabarti S. Testing and validation of power system dynamic state estimators using real time digital simulator (RTDS). IEEE Trans Power Syst 2016;31(3):2338–47. http://dx.doi.org/10.1109/TPWRS.2015.2453482.

[39] Valverde G, Terzija V. Unscented Kalman filter for power system dynamic state estimation. IET Gener, Transm Distrib 2011;5(1):29–37.

[40] Akhlaghi S, Zhou N, Huang Z. Hybrid approach for estimating dynamic states of synchronous generators. IET Gener, Transm Distrib 2019;13(5):669–78. http://dx.doi.org/10.1049/IET-GTD.2018.5074.

[41] Ćetenović D, Ranković A, Zhao J, Jin Z, Wu J, Terzija V. An adaptive method for tuning process noise covariance matrix in EKF-based three-phase distribution system state estimation. Int J Electr Power Energy Syst 2021;132:107192. http://dx.doi.org/10.1016/j.ijepes.2021.107192.

[42] Ćetenović DN, Ranković AM. Optimal parameterization of Kalman filter based three-phase dynamic state estimator for active distribution networks. Int J Electr Power Energy Syst 2018;101:472–81. http://dx.doi.org/10.1016/J.IJEPES.2018.04.008.

[43] Falcao DM, Cooke PA, Brameller A. Power system tracking state estimation and bad data processing. IEEE Trans Power Appar Syst 1982;PAS-101(2):325–33. http://dx.doi.org/10.1109/TPAS.1982.317110.

[44] Nishiya K-I, Takagi H, Hasegawa J, Koike T. Dynamic state estimation for electric power systems—Introduction of a trend factor and detection of innovation processes. Electr Eng Japan 1976;96(5):79–87. http://dx.doi.org/10.1002/eej.4390960511, URL https://onlinelibrary.wiley.com/doi/abs/10.1002/eej.4390960511.

[45] Nishiya K-I, Takagi H, Hasegawa J, Koike T. Dynamic state estimation including detection of innovation process for electric power systems. Electr Eng Japan 1978;98(1):52–61. http://dx.doi.org/10.1002/eej.4390980108.

[46] Caro E, Conejo AJ, Mínguez R. Power system state estimation considering measurement dependencies. IEEE Trans Power Syst 2009;24(4):1875–85. http://dx.doi.org/10.1109/TPWRS.2009.2030385.

[47] Wang S, Zhao J, Huang Z, Diao R. Assessing Gaussian assumption of PMU measurement error using field data. IEEE Trans Power Deliv 2018;33(6):3233–6. http://dx.doi.org/10.1109/TPWRD.2017.2762927.

[48] Li Y, Li J, Qi J, Chen L. Robust cubature Kalman filter for dynamic state estimation of synchronous machines under unknown measurement noise statistics. IEEE Access 2019;7:29139–48. http://dx.doi.org/10.1109/ACCESS.2019.2900228.

[49] Martínez-Parrales R, Fuerte-Esquivel CR, Alcaide-Moreno BA. Analysis of bad data in power system state estimation under non-Gaussian measurement noise. Electr Power Syst Res 2020;186:106424. http://dx.doi.org/10.1016/J.EPSR.2020.106424.

[50] Usman MU, Faruque MO. Validation of a PMU based fault location identification method for smart distribution network with photovoltaics using real-time data. IET Gener Transm Distrib 2018;12. http://dx.doi.org/10.1049/iet-gtd.2018.6245.

[51] Naglic M, Popov M, Van Der Meijden MA, Terzija V. Synchro-measurement application development framework: An IEEE standard C37.118.2-2011 supported MATLAB library. IEEE Trans Instrum Meas 2018;67(8):1804–14. http://dx.doi.org/10.1109/TIM.2018.2807000.